Hindawi
Advances in High Energy Physics
Volume 2020, Article ID 5074618, 11 pages
https://doi.org/10.1155/2020/5074618

Research Article

Conditions for Vacuum Instability in Holographic Theories with Dilaton Field

Sara Tahery,[1] **Sreeraj Nair**,[1] **and Pengming Zhang**[2]

[1]*Institute of Modern Physics, Chinese Academy of Sciences, Lanzhou, China*
[2]*School of Physics and Astronomy, Sun Yat-sen University, Zhuhai, China*

Correspondence should be addressed to Sara Tahery; s.tahery@impcas.ac.cn

Received 17 October 2019; Accepted 27 December 2019; Published 9 January 2020

Academic Editor: Torsten Asselmeyer-Maluga

We investigate the vacuum instability in the presence of dilaton field in a holographic setup. Although the dilaton is a bulk field, it leads to the vacuum instability on the boundary. We show that the whole process crucially depends on the probe brane position and as well on the radial coordinate so that the effects of dilaton scale parameter in different regions of the bulk or for different probe brane positions are different. We also observe that in our study, the temperature can strengthen the effect of scale parameter in reducing the potential barrier. Finally, we show that this Schwinger-like effect, although is interesting by itself, does not produce a considerable pair production rate.

1. Introduction

Pair production in the presence of an external electric field is known as the Schwinger effect in nonperturbative quantum electrodynamics (QED) [1]. Due to this phenomenon, when the external field is strong enough, the virtual electron-positron pair becomes a real particle. In other words, vacuum is destroyed in the presence of such a field.

Although this context had been considered in QED first, it is not restricted to it anymore. It has been extended to quantum chromodynamics (QCD) and even higher-dimensional objects like strings and branes [2]. As an interesting example, it has been considered in a gravitational wave background while the electric field was replaced by the gravitational wave background and the electron/positron field quanta were replaced by massless scalar photons [3]. In other words, nowadays, the Schwinger effect is not restricted to QED, external electric field, and electron-positron pair production, but any kind of vacuum decay due to pair production in the presence of any external field stands for the Schwinger effect.

Potential analysis plays an important role in vacuum stability. The main setup of our current work is based on considering vacuum decay process by diminishing the potential barrier. Before going to the main subject, we mention Schwinger effect which gives us the strategy of our computation, but we will discuss the important differences between this effect (in its known form) and the current work in upcoming calculations as well.

In the context of QED, the potential analysis estimated by the static potential includes the Coulomb interaction between the particles in addition to an energy Ex, where x is a separating distance of the virtual pair and E is an external electric field [4]. Generally, the total potential is calculated by the Lagrangian integration over the internal distance of the pair, in addition to a term coming from the external field energy. This is the strategy: the internal energy of the virtual pair leads to a potential barrier. When the virtual pair gets a greater energy than the rest energy from an external field, it becomes real. So, for the creation of a real pair which corresponds to the vacuum decay, the external field should reach to a critical value, where the vacuum becomes totally unstable.

In QED, increasing electric field can destroy the potential barrier and finally vacuum decays. Accordingly, one can expect that in any kind of Schwinger effect, increasing

external field results in destroying the potential barrier. When the external field is small, the potential barrier is present and the pair production is a tunneling process. The potential barrier diminishes as the external field increases. At a critical value of the field, the potential barrier vanishes completely and the pair production is catastrophic [2]. From string theory point of view, this critical value is regarded as string behaviour in ultraviolet (UV) completion of the string [5, 6].

One strong tool to investigate Schwinger effect in string context or higher-dimensional objects is AdS/CFT which is a correspondence describing a relation between a d-dimensional conformal field theory (CFT) and a $(d+1)$ dimensional string theory in anti-de Sitter (AdS) space [7]. This is a powerful mathematical tool to investigate about strongly correlated systems [8–10]. Extra dimension in the AdS side leads to using the energy scale of the CFT side on the boundary. Although QCD is not a CFT exactly, in recent decades, AdS/QCD has been considered a useful approach to study an analytic semiclassical model for strongly coupled QCD. It has scale invariance, dimensional counting at short distances, and color confinement at large distances. This theory describes the phenomenology of hadronic properties and demonstrates their ability to incorporate such essential properties of QCD-like confinement and chiral symmetry breaking. From the AdS/CFT point of view, the AdS_5 plays an important role in describing QCD phenomenon, so it is called AdS/QCD [11–13].

Many works have been done about Schwinger effect in a holographic setup related to quark-antiquark pair production as follows, the creation rate of the quark pair in $N=4$ SYM theory was obtained in [14] and based on that, the holographic Schwinger effect was calculated in various systems [2, 4, 15–25]. Also, the vacuum decay rate is regarded as the creation rate of the quark-antiquark in $N=2$ supersymmetric QCD (SQCD) [26]. In Ref. [27], electrostatic potentials in the holographic Schwinger effect have been analyzed for the finite temperature and temperature-dependent critical field cases to find agreement with the full form Dirac-Born-Infeld (DBI) result. In Ref. [28], tunneling pair creation of W-Bosons by an external electric field on the Coulomb branch of $N=4$ supersymmetric Yang-Mills theory has been studied and found that the pair creation formula has an upper critical electric field beyond which the process is no longer exponentially suppressed.

Light-front holographic QCD [29, 30] is a model theory, which tries to explain nonperturbative features of quantum field theory for strong interactions, QCD. In order to get some insight into the structure of the most interesting phenomena, one has to make specific models and approximations. An important approach is the semiclassical approximation of a quantum field theory. The basis of light-front holographic QCD is the "holographic principle" which states that certain aspects of a quantum field theory in four space-time dimensions can be obtained as limiting values of a five-dimensional theory as it is mentioned before. In light-front holographic QCD (LFHQCD), one chooses a bottom-up approach; that is, one modifies the five-dimensional classical theory in such a way as to obtain from this modified theory and the holographic principle realistic features of hadron physics [31]. In LFHQCD, the action is an invariant action, modified by a dilaton term $e^{\varphi(z)}$ as

$$S_{\text{eff}} = \int d^d x dz \sqrt{g} e^{\varphi(z)} g^{N_1 N_1'} \cdots g^{N_j N_j'} \cdot \left(g^{MM'} D_M \Phi^*_{N_1 \cdots N_j} D_{M'} \Phi_{N_1' \cdots N_j'} - \mu^2_{\text{eff}}(z) \Phi^*_{N_1 \cdots N_j} \Phi_{N_1' \cdots N_j'} \right), \tag{1}$$

according to the dictionary between the AdS result and the LFH, the potential is related to the dilaton field in the effective AdS_5 action. The corresponding metric with the mentioned action is an asymptotic AdS_5 metric modified by a dilaton field $\varphi(z)$. It is only a function of the holographic variable z which vanishes in the conformal limit $z \to 0$. In AdS_5, this unique z dependence of the dilaton field allows the description of the bound-state dynamics in terms of a one-dimensional wave equation. It also enables one to establish a map to the semiclassical one-dimensional approximation to light-front QCD given by the frame-independent light-front Schrödinger equation. It has been found that the dilaton profile has the specific form $\varphi(z) = -\lambda z^2$ [31] which leads to linear Regge trajectories and avoids the ambiguities in the choice of boundary conditions at the infrared wall [30]. The spectrum can only be described by choosing $\lambda > 0$. Thus, in this work, we consider the dilaton profile as $\varphi(z) = -\lambda z^2$ with positive λ.

In Ref. [32], one of the authors of this work considered vacuum instability in a deformed AdS in the presence of an electric field. In the current work, our motivation is to consider vacuum instability by this holographic model and without any external electric field. This holographic model is important from two different points of view. First, it stands for light-front holographic approach which has been mentioned before. Second, it can be considered a deformed AdS where one deforms the AdS by the second correction of the radial coordinate [33], to discuss on some asymptotically AdS behaviour of the theory. In the next section, we will represent such a metric with an estimate of the quadratic correction of the radial coordinate based on gauge/string duality. In References [33, 34], it is written that in QCD analysis of the two-current correlator, the first coefficient can be calculated perturbatively, while the second coefficient (quadratic correction) is not easy to be found. Then, it should be estimated based on some data. Correspondingly, in gauge/gravity duality, in models with the slightly deformed AdS_5 metric, one can find some results fit better to QCD which remains to be seen. Here, we only addressed the main motivation and avoided opening many details of discussion, so interested readers can refer to the main references. We will focus on the first point of view keeping in our mind that our results will cover deformed AdS/QCD too [34]. So, starting by the soft-wall LFH metric, we are interested in studying vacuum decay process.

The process starts from "turning on the λ" which means to consider the nonzero value of this scale parameter. As λ increases, we expect that the potential barrier diminishes.

Therefore, one interprets that the potential barrier is supposed to be vanished by a "large enough value of λ." Although Schwinger effect has been considered by external electric field and magnetic field before, the most important difference of the current work is that the vacuum decay initiates from inside the metric. Briefly, λ is responsible for vacuum decay and pair production; thus, it has the main role in this process. This is a goal to see the effects of space-time specifications during vacuum decay.

With all above explanations, we represent this paper as follows. In Section 2, we consider vacuum decay by dilaton field at zero temperature. Proceeding by finite temperature, we follow the study in Section 3. In Sections 4 and 5, the pair production rate for both zero and thermal cases is discussed. Section 6 is the numerical strategy, and our conclusion and results will be represented in Section 7.

2. Potential Analysis at Zero Temperature

Considering LFH metric at zero temperature, we analyze the potential initiated by the dilaton field. According to the holographic setup in [27], we will derive the total potential from the action. The LFH metric is written as

$$ds^2 = \frac{R^2}{z^2} h(z) \left(-dt^2 + \sum_{i=0}^{3} dx_i^2 + dz^2 \right) + R^2 d\Omega_5^2, \quad h(z) = e^{-\lambda z^2}, \tag{2}$$

where R is the radius of space which is related to the slope parameter and coupling via $R^2 = \alpha' \sqrt{\lambda}$, with $\alpha' = l_s{}^2$ where l_s is the string scale. Moreover, $d\Omega_5^2$ is the metric of a five-dimensional sphere.

The potential of the produced pair particle is obtained using the expectation value of the Wilson loop. The loop corresponds to a trajectory of test particles with infinite heavy mass, and the expectation value corresponds to the area of a string worldsheet attached to the Wilson loop [35, 36]. Thus, in order to study by AdS/CFT, the area of the rectangular Wilson loop on the probe D3-brane evaluates classical action of a string attached to the probe D3-brane [28]. The Nambu-Goto string action is given by

$$S = T_F \int d\tau d\sigma \mathscr{L} = T_F \int d\tau d\sigma \sqrt{\det G_{ab}}, \tag{3}$$

where

$$G_{ab} \equiv \frac{\partial x^\mu}{\partial \sigma^a} \frac{\partial x^\nu}{\partial \sigma^b} g_{\mu\nu} \tag{4}$$

is the induced metric and $\sigma^a = (\tau, \sigma)$ are worldsheet coordinates and $T_F = 1/2\pi\alpha'$ is the string tension. From relation (2), we have

$$g_{ab} = \text{diag} \left(-\frac{R^2}{z^2} e^{-\lambda z^2}, \frac{R^2}{z^2} e^{-\lambda z^2} \right). \tag{5}$$

It is useful to choose the static gauge, $x^0 = \tau$, and $x^1 = \sigma$. So, the radial direction $z(\sigma)$ depends only on σ in classical solution. Therefore, the Lagrangian is

$$\mathscr{L} = \frac{R^2}{z^2} e^{-\lambda z^2} \sqrt{1 + \left(\frac{dz}{d\sigma} \right)^2}. \tag{6}$$

From the equation of motion, one can find

$$\frac{\partial \mathscr{L}}{\partial (\partial_\sigma z)} \partial_\sigma z - \mathscr{L} = C_1, \tag{7}$$

where C_1 is an arbitrary constant, and this yields to the following relation:

$$\frac{R^2}{z^2} \frac{e^{-\lambda z^2}}{\sqrt{1 + (dz/d\sigma)^2}} = C_2, \tag{8}$$

where C_2 is an arbitrary constant. The important boundary condition at $\sigma = 0$ imposes

$$\frac{dz}{d\sigma} = 0, \quad z = z_*, \tag{9}$$

where z_* is the turning point, which means the deepest position of the string in the bulk. Therefore, we yield to the following differential equation:

$$\frac{dz}{d\sigma} = \sqrt{\frac{z_*^4}{z^4} e^{-2\lambda \left(z^2 - z_*^2 \right)} - 1}. \tag{10}$$

Thus, the separation length of the test particles on the probe brane is

$$x = \int_{z_0}^{z_*} \frac{dz}{\sqrt{(z_*^4/z^4) e^{-2\lambda (z^2 - z_*^2)} - 1}}, \tag{11}$$

where z_0 is the probe brane position. We will use this length in considering behaviour of potential later. From the Lagrangian (6), the potential of the produced pair particle is given by

$$V = 2T_F \int_0^{x/2} dx \mathscr{L} = 2T_F R^2 z_*^2 \int_{z_0}^{z_*} \frac{1}{z^4} \frac{e^{-\lambda \left(2z^2 - z_*^2 \right)}}{\sqrt{(z_*^4/z^4) e^{-2\lambda (z^2 - z_*^2)} - 1}} dz. \tag{12}$$

Before studying this potential, it is useful to introduce another quantity as critical dilaton field. The critical value of the dilaton field corresponds to the value at which the potential barrier is destroyed and pair production begins. According to the metric and by considering the fact that

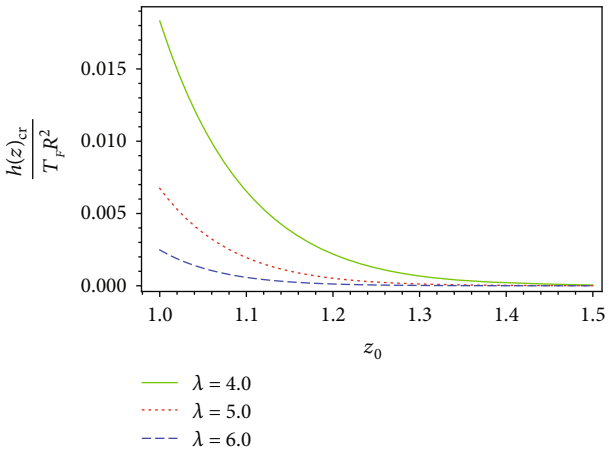

FIGURE 1: Considering the critical field against probe brane position, at zero temperature and for different values of scale parameter.

the critical field is interpreted as string tension σ_{string} in the string theory side [37],

$$\sigma_{\text{string}} = T_F \sqrt{-g_{00} g_{11}} IR. \tag{13}$$

Then, the result at zero temperature is

$$\sigma_{\text{string}} = T_F \frac{R^2}{z_0^2} e^{-\lambda z_0^2}, \tag{14}$$

which corresponds to

$$h(z)_{\text{cr}} = T_F \frac{R^2}{z_0^2} e^{-\lambda z_0^2}. \tag{15}$$

We define a dimensionless value as the ratio of the field to its critical value as

$$\alpha = \frac{h(z)}{h(z)_{\text{cr}}} = \frac{e^{-\lambda z^2}}{T_F \left(R^2/z_0^2\right) e^{-\lambda z_0^2}} = \frac{z_0^2}{T_F R^2} e^{-\lambda\left(z^2 - z_0^2\right)}. \tag{16}$$

Based on previous works on Schwinger effect, we expect that when α is unity, the pair production process gets started [19, 27]. We will see that this is not a sufficient condition for pair production in this work.

It is worth mentioning that the space-time metric parameters and the brane configuration all affect the Schwinger effect considered here. Figure 1 considers the critical value of the field as a function of z_0. Clearly, with increasing z_0, the critical value of the field decreases. So when the probe brane is near the boundary ($z = 0$), a larger value of the critical field is obtained for pair production. In addition, greater λ corresponds to a smaller value of the critical field at the same z_0. This behaviour has an exception in the region far from the boundary where different plots with different λ are coincident. It means that when the probe brane is far from the boundary, the scale parameter has no significant effect on the critical field.

In Figure 2, based on the relation between α and λ, behaviour of α has been considered with respect to the scale parameter λ, for different values of z_0. By choosing fixed probe brane position, one can consider effects of scale parameter and position of probe brane on α. Obviously, when the probe brane is in the near-boundary region, $\alpha = 1$ is obtainable in a limited region near it and for a wide range of λ values as we can see in plot (a). By increasing z_0, in plot (b), the condition $\alpha \geq 1$ is satisfied almost along the z coordinate. With increasing z_0, large values of scale parameter lead to large values of α.

In Figure 3, we show the two-dimensional (2D) cross-section of Figure 2 for fixed probe brane position $z_0 = 2$. We observe a critical point at $z = z_0$, where α is independent of λ. After the critical point, α decreases with increasing λ. In other words, scale parameter affects pair production and also the probe brane position is important. In addition, the behaviour depends on the distance along the z axis.

Figure 4 shows the potential for different λ values with a fixed probe brane position. We observe that $\alpha \geq 1$ is not a sufficient condition for pair production; we need large values of λ to overcome the potential barrier. Table 1 shows the maximum values of V_{tot} and x for different values of λ. One notices that for large λ, the potential vanishes. So we can conclude that to create a pair the necessary condition is to have large λ.

3. Potential Analysis at Finite Temperature

In this section, potential analysis will be considered at finite temperature. The modified thermal metric is given by

$$ds^2 = \frac{R^2}{z^2} h(z) \left(-f(z) dt^2 + \sum_{i=1}^{3} dx_i^2 + \frac{1}{f(z)} dz^2 \right) + R^2 d\Omega_5^2, \tag{17}$$

where

$$f(z) = 1 - \left(\frac{z}{zh}\right)^4, \quad h(z) = e^{-\lambda z^2}. \tag{18}$$

The horizon is located at $z = z_h$, where $z_0 < z_* < z_h$, and the temperature of the black hole is written as $T = 1/\pi z_h$, so zero temperature limit $z_h \to \infty$ and $f(z) \to 1$ have been discussed in the previous section. The Lagrangian is given by

$$\mathscr{L} = \frac{R^2}{z^2} e^{-\lambda z^2} \sqrt{\left(1 - \frac{z^4}{z_h^4}\right) + \left(\frac{dz}{d\sigma}\right)^2}. \tag{19}$$

By using the equation of motion, one can find

$$\frac{R^2}{z^2} \frac{e^{-\lambda z^2}\left(1 - \left(z^4/z_h^4\right)\right)}{\sqrt{\left(1 - \left(z^4/z_h^4\right)\right) + (dz/d\sigma)^2}} = C, \tag{20}$$

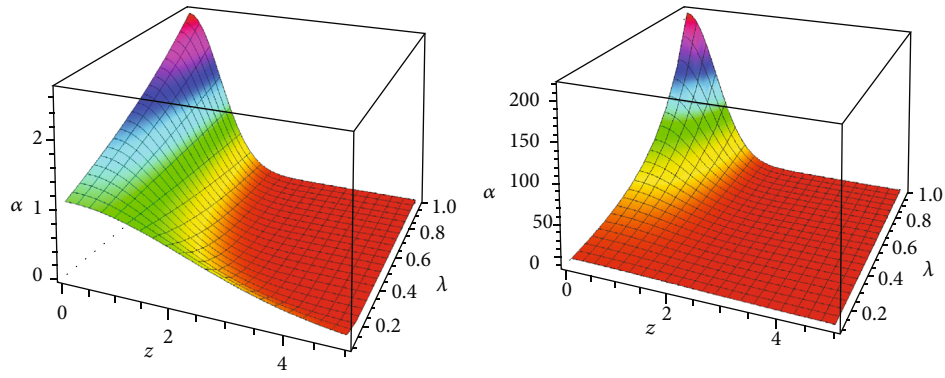

FIGURE 2: Considering pair production parameters versus each other in a 3D plot, at zero temperature and fixed value of probe brane position at (a) $z_0 = 1$ and (b) $z_0 = 2$.

which yields to the following differential equation:

$$\frac{dz}{d\sigma} = \sqrt{\frac{z_*^4}{z^4} e^{-2\lambda\left(z^2 - z_*^2\right)} \frac{\left(1 - \left(z^4/z_h^4\right)\right)^2}{\left(1 - \left(z_*^4/z_h^4\right)\right)} - \left(1 - \frac{z^4}{z_h^4}\right)}. \quad (21)$$

So, the internal separation length of the pair particles is obtained as

$$x = \int_{z_0}^{z_*} \frac{dz}{\sqrt{\left(z^4/z^4\right) e^{-2\lambda\left(z^2 - z_*^2\right)} \left(\left(1 - \left(z^4/z_h^4\right)\right)^2 / \left(1 - \left(z_*^4/z_h^4\right)\right)\right) - \left(1 - \left(z^4/z_h^4\right)\right)}}, \quad (22)$$

and the total potential is found as

$$V = 2T_F \int_0^{x/2} dx \mathscr{L} = 2T_F R^2 z_*^2 \int_{z_0}^{z_*} \frac{1}{z^4} \frac{e^{-\lambda\left(2z^2 - z_*^2\right)}}{\sqrt{\left(z_*^4/z^4\right) e^{-2\lambda\left(z^2 - z_*^2\right)} - \left(\left(1 - \left(z_*^4/z_h^4\right)\right) / \left(1 - \left(z^4/z_h^4\right)\right)\right)}} dz. \quad (23)$$

Similar to the last section, there is a critical value of the field, in which the pair production process starts. The thermal metric results in [37]

$$h(z)_{\mathrm{cr}} = T_F \frac{R^2}{z_0^2} e^{-\lambda z_0^2} \sqrt{1 - b^4}, \quad (24)$$

where $b = z_0/z_h$. Using (24), one can derive the α in the thermal case as

$$\alpha = \frac{h(z)}{h(z)_{\mathrm{cr}}} = \frac{z_0^2}{T_F R^2} \frac{e^{-\lambda\left(z^2 - z_0^2\right)}}{\sqrt{1 - b^4}}. \quad (25)$$

According to this ratio, we proceed by considering it in different temperatures and at fixed scale parameter in Figure 5(a). At the boundary, α has its maximum value. Moving along the radial coordinate, α decreases significantly. This manner is obvious in the thermal case, similar to what we have considered in Figure 3 at zero temperature. We observe that α increases with increasing temperature, but far from the boundary region, α becomes independent of temperature. The behaviour of α at fixed temperature but with different scale parameters is shown in Figure 5(b) where we find the effects of λ on α according to the region. We observe a critical point at $z = z_0$ similar to the zero temperature case at which α becomes independent of λ. The greater λ leads to larger α from the boundary up to $z = z_0$ in the bulk; then, this behaviour changes clearly in reverse. It can be interpreted as the effect of scale parameter near the boundary is completely different with the near-horizon region.

As it is represented in Figure 6, the critical field has a monotonous manner in low temperature. On the one hand, by increasing the temperature, the critical field falls down. On the other hand, increasing scale parameter decreases the value of the critical field. So, at the same temperature, greater λ leads to a smaller critical field which should be obtained for the starting point of the pair production. When the probe brane is in the near-horizon limit, all the plots with different λ coincide and increasing λ does not have any effect anymore.

According to (23), the total potential has been shown in Figure 7. We study the total potential at fixed value of scale parameter in Figure 7(a) and at fixed temperature in Figure 7(b). We observe that in Figure 7(a) increasing value of b slightly reduces the potential as seen in Table 2 and in

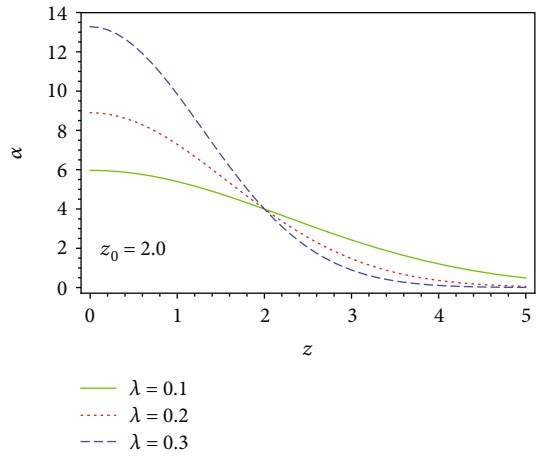

Figure 3: Considering behaviour of α along the z axis at zero temperature with different values of scale parameter.

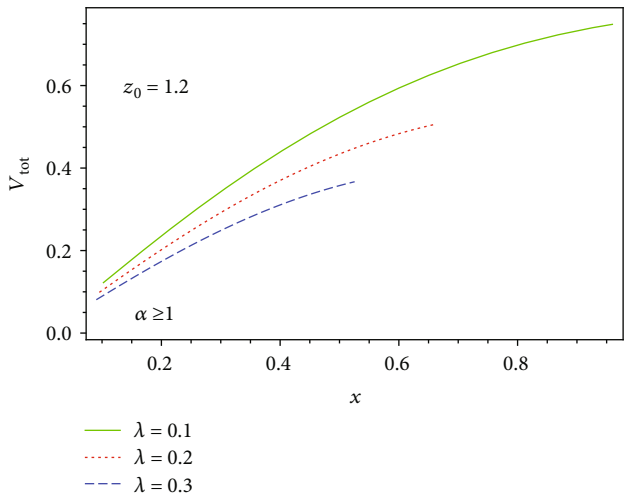

Figure 4: Considering behaviour of potential during pair production at zero temperature.

Table 1: Maximum values of V_{tot} and x for different values of λ for $z_0 = 1.2$.

λ	x	V
0.1	0.96	0.75
0.5	0.38	0.21
1.0	0.24	6.59×10^{-2}
2.0	0.13	9.18×10^{-3}
5.0	0.06	5.63×10^{-5}

Figure 7(b) increasing value of λ has the effect of reducing the potential barrier. Although increasing both λ and b reduces the potential, in comparison, the effect of b is not as significant as λ. Thus, we can say that the effect of temperature is to just strengthen the effect of λ.

4. Effects of Scale Parameter on Pair Production Rate at Zero Temperature

The production rate P (per unit time and volume) is evaluated by computing the expectation value of a circular Wilson loop on the probe brane in the holographic description with the string action [19]. According to [17], we have to find the minimal action, because the pair production probability is given by $\omega \propto e^{-S_{min}}$. In other words, based on [14], exponential dependence of the probability rate is given by the minimum of the string effective action.

By the holographic setup, we should consider the action in both zero and finite temperature cases. Deriving the differential equation of motion, we will find numerically the $z(\sigma)$ satisfying the related boundary conditions. Then, we will evaluate the action at this specific $z(\sigma)$. So, just to remind, the action at zero temperature is defined as

$$S = 2\pi T_F R^2 \int_0^x d\sigma \frac{1}{z^2} e^{-\lambda z^2} \sqrt{1 + z'^2}. \tag{26}$$

From relation (6) and by the Euler-Lagrange equation,

$$\frac{d}{d\sigma}\left(\frac{\partial \mathscr{L}}{\partial z'}\right) - \frac{\partial \mathscr{L}}{\partial z} = 0, \tag{27}$$

the following differential equation is obtained:

$$zz'' + 2\left(1 + z'^2\right)\left(1 + \lambda z^2\right) = 0, \tag{28}$$

where $z = z(\sigma)$ and $z' = dz(\sigma)/d\sigma$. Now, we should find numerically $z(\sigma)$ satisfying these differential equations and conditions:

$$\begin{aligned} z(0) &= z_*, \\ z(\sigma_0) &= z_0. \end{aligned} \tag{29}$$

After finding $z(\sigma)$, the classical action should be evaluated numerically.

In Figure 8, the pair production rate in the Schwinger effect at zero temperature is represented. Pair production rate is also under the effect of probe brane position intensively, as a greater value of z_0 makes a larger pair production rate. However, all the plots are definable in a specific width of the α before falling down. When the pair production starts, the rate decreases with increasing α immediately. In other words, although the ratio of the field to its critical value is increasing, it will not work as an effective factor of increasing the pair production rate; on the contrary, the pair production rate decreases immediately, and in this case, there is no catastrophic pair production. One can interpret that pair production is considerable in a special large enough value of λ. Vacuum stability in both limits $\lambda \to 0$ and $\lambda \to \infty$ is in agreement with the stability of vacuum described by AdS_5.

In Figure 9, the pair production rate of the process is represented. We can see that maximum values of the rate is obtained when we increase λ. In a large enough value of scale

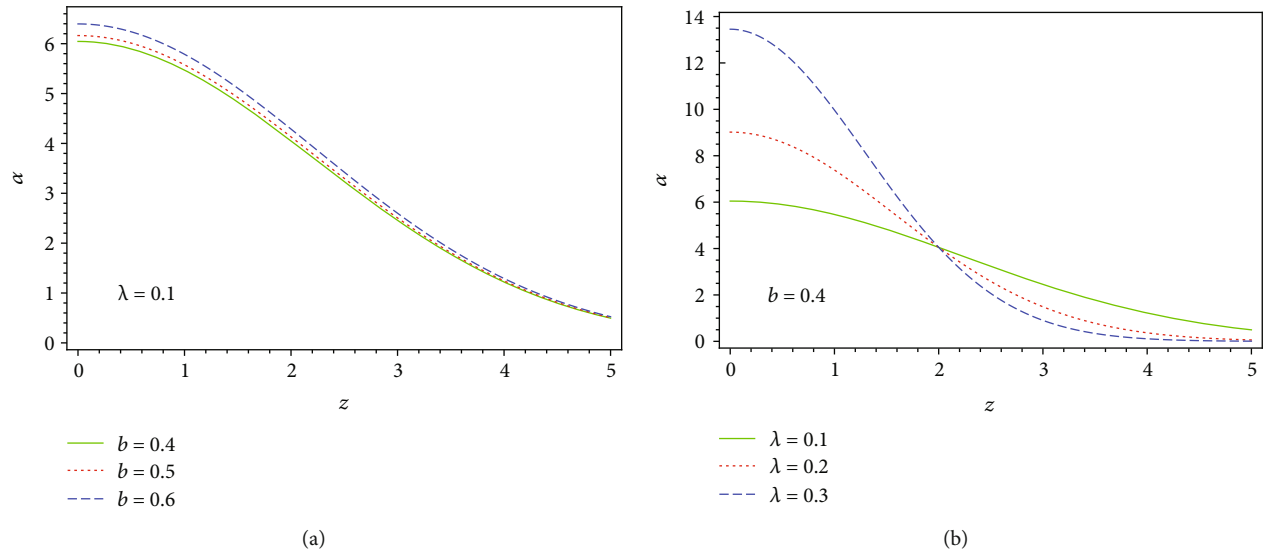

Figure 5: Considering α versus z coordinate at (a) different temperatures and (b) different scale parameters.

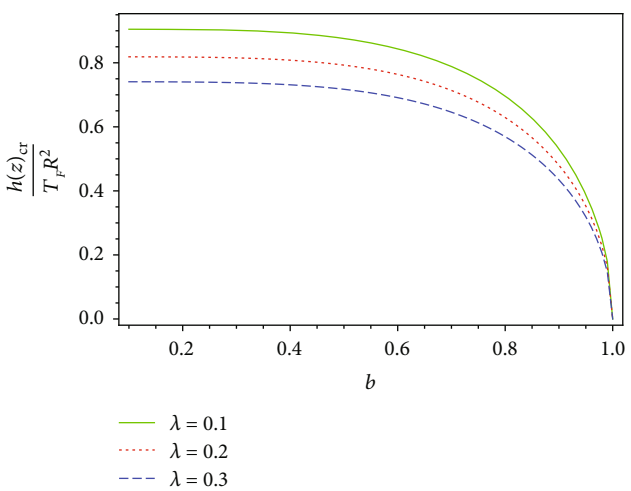

Figure 6: Considering behaviour of the critical field versus temperature.

parameter, the potential barrier will be destroyed, that is, in agreement with our discussion in the last section. Studying this plot, we find that from tunneling process to pair production, this is what happens: during tunneling process, there is a maximum value of pair production rate with an approximately monotonous manner with respect to α. After vacuum decay, still greater scale parameter leads to larger rate. But this rate falls down after a while more intense than for smaller λ cases. Therefore, when λ is large enough to destroy the potential barrier, pair production via Schwinger effect happens in a short range of α, and thereafter, its rate fades. The common point in these two plots is that there is no catastrophic pair production since the creation of the pair has a decreasing behaviour from its maximum value at the starting point to zero. So, this kind of process will not continue as long as α is increasing. So we do not consider pair production forever, and no catastrophic pair production happens.

5. Effects of Scale Parameter on Pair Production Rate at Finite Temperature

Considering the thermal case from (19), the action is defined as

$$S = 2\pi T_F R^2 \int_0^x d\sigma \frac{1}{z^2} e^{-\lambda z^2} \sqrt{f(z) + z'^2}. \tag{30}$$

From the Euler-Lagrange equation, the differential equation is found as

$$\begin{aligned} zz'' f(z) - zz'^2 \frac{df}{dz} - \frac{1}{2} zf(z) \frac{df}{dz} \\ + 2\left(f(z) + z'^2\right) f(z)\left(1 + \lambda z^2\right) = 0. \end{aligned} \tag{31}$$

Similar to the zero temperature case, classical action at the satisfying $z(\sigma)$ value should be evaluated. Behaviour of the pair production rate at finite temperature has been considered in Figure 10. Here, fixed value of scale parameter and different temperatures are considered. One can follow from tunneling process to pair production. The pair production rate decreases with increasing α, while greater temperature leads to greater pair production rate at the same scale parameter. In addition, by increasing the temperature, the pair production rate descends with the smaller slope. It means that at a fixed λ, although the pair production rate has a decreasing behaviour similar to the zero temperature case, the temperature can strengthen this rate as larger temperature results in greater pair production rate.

Comparative with Figure 9, the pair production rate has been represented at different values of scale parameter and finite temperature in Figure 11. As we saw in the zero temperature case, the maximum value of pair production rate is produced when one manipulates λ to increase, as much as possible. In other words, the largest scale parameter leads to greater rate of the pair creation. However, such a rate is

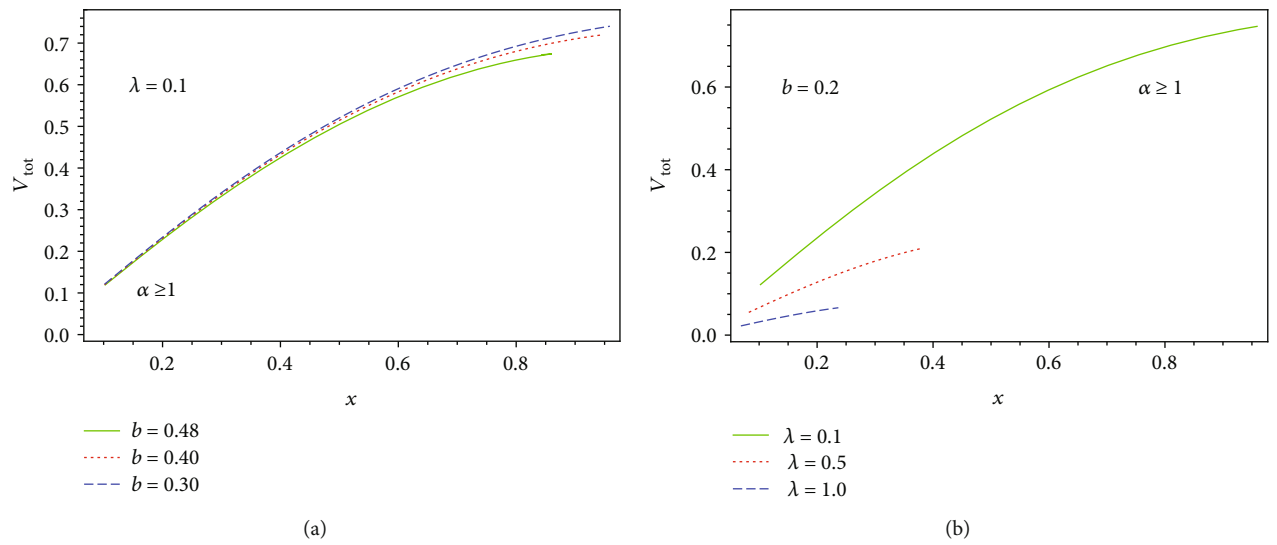

Figure 7: Considering the total potential in the pair production process, at (a) different values of temperature and (b) different values of λ.

Table 2: Maximum values of V_{tot} and x for different values of b for $\lambda = 0.5$.

b	x	V
0.2	0.38	0.21
0.4	0.39	0.21
0.6	0.42	0.20
0.8	0.26	0.14
0.98	0.09	0.02

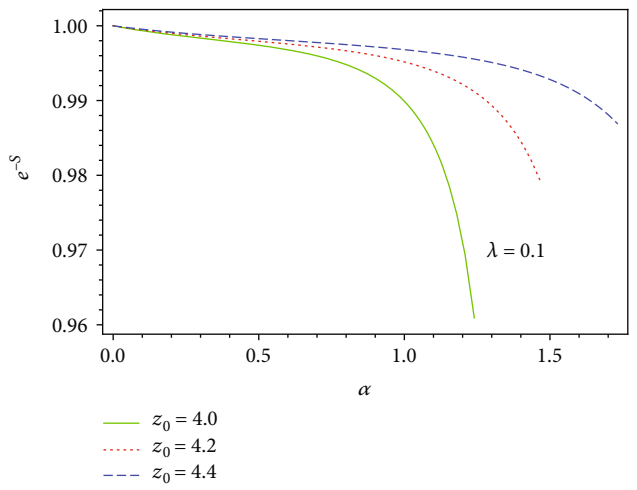

Figure 8: Considering pair production rate at zero temperature and fixed value of scale parameter and different probe brane positions.

accessible in a limited range of α and it falls down intensively as it decreases with increasing α. This manner is common in both zero and finite temperature cases. So the temperature does not affect the pair production process significantly

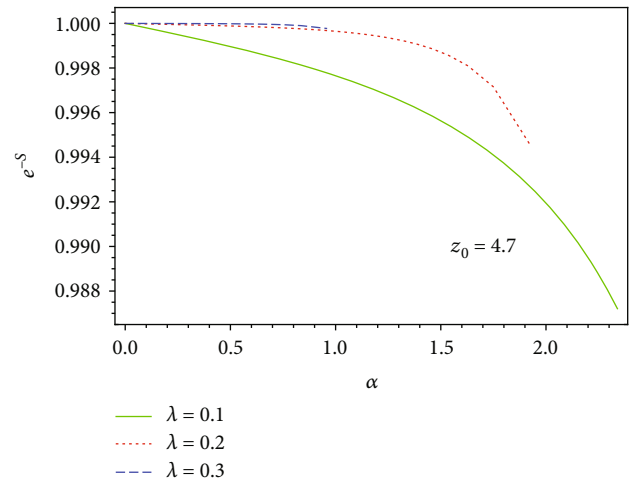

Figure 9: Considering pair production rate at zero temperature and fixed probe brane position and different large values of scale parameter.

while probe brane position and scale parameters do that meaningfully. In addition, in both zero temperature and finite temperature cases, pair production rate has a decreasing behaviour just after starting the process. Temperature strengthens the pair production rate as we saw in Figure 9, but it can change the decreasing behaviour, and still there is no catastrophic pair production in this Schwinger-like effect.

At the end of this section, one point should be mentioned based on what we have seen so far. When vacuum decays, the particle and antiparticle should be created at the same time. Naturally, they are in short distance from each other, especially in our case that one of the main results is that the system tends to go back to stability immediately. So, according to our previous results, long distance cannot be considered in our case.

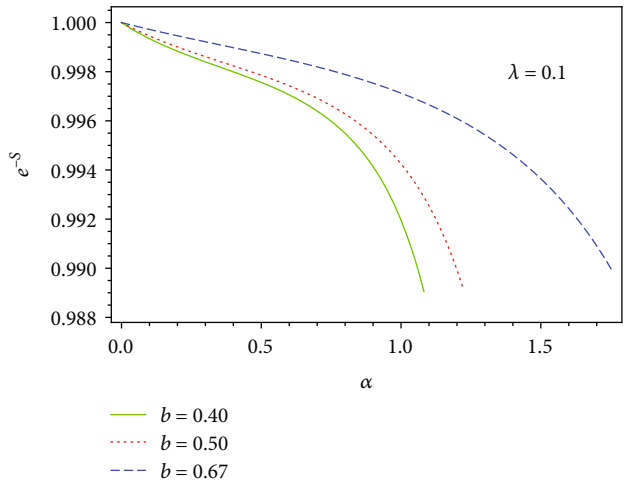

FIGURE 10: Considering pair production rate at finite temperature, different probe brane positions, and fixed value of scale parameter.

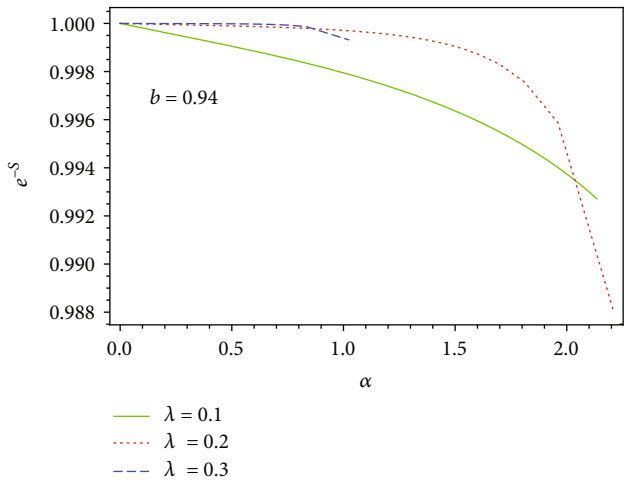

FIGURE 11: Considering pair production rate at finite temperature and fixed probe brane position and different large values of scale parameter.

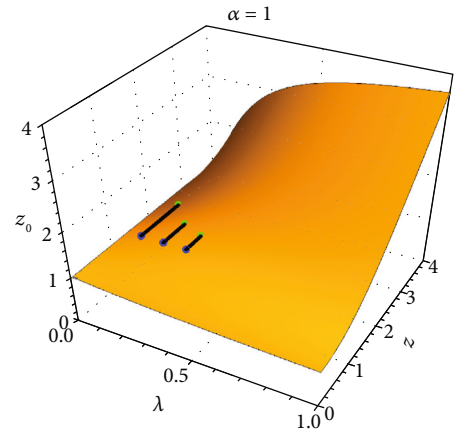

FIGURE 12: Surface plot satisfying the condition $\alpha = 1$. The region above and below the surface corresponds to $\alpha > 1$ and $\alpha < 1$, respectively. The black lines show the range of integration for $\alpha \geq 1$. The blue and green dots correspond to the value of $z_*^{\min}$ and $z_*^{\max}$, respectively.

TABLE 3: Parameter values used in Figure 4.

λ	z_0	$z_*^{\min}$	$z_*^{\max}$
0.10	1.2	1.21	2.29
0.20	1.2	1.21	1.84
0.30	1.2	1.21	1.65

TABLE 4: Parameter values for finite temperature potential plots.

	λ	z_0	z_h	b	$z_*^{\min}$	$z_*^{\max}$
Figure 7(a)	0.10	1.2	2.5	0.48	1.21	2.31
	0.10	1.2	3.0	0.40	1.21	2.28
	0.10	1.2	4.0	0.30	1.21	2.26
Figure 7(b)	0.10	1.2	6	0.20	1.21	2.26
	0.50	1.2	6	0.20	1.21	1.47
	1.00	1.2	6	0.20	1.21	1.34

6. Numerical Strategy

The integration for x and V, respectively, is solved numerically to generate the plots shown in Figures 4 and 7. We choose the value of $z_0 = 1.2$ which falls in the region $\alpha \geq 1$ as seen in Figure 12.

The upper limit of the integration is varied over a range from $z_*^{\min}$ to $z_*^{\max}$ to generate the data for the plots. The value of $z_*^{\min}$ and $z_*^{\max}$ used is shown in Table 3 along with other parameters.

The value of $z_*^{\max}$ is the value at which $\alpha(\lambda, z_0, z_*^{\max}) = 1$. The integration range for each λ value corresponding to $\alpha \geq 1$ is shown in Figure 12 as a black line were the blue and green dots correspond to $z_*^{\min}$ and $z_*^{\max}$, respectively. We see that the green dots are points on the surface plot $\alpha = 1$.

The region beyond the green dots corresponds to $\alpha < 1$, and hence, they set the maximum value for the upper limit in the integration of x and V. We extend the same numerical strategy for the finite temperature plots. The value of the parameters for the finite temperature potential plots is shown in Table 4.

The pair production plots for zero temperature in Section 4 are produced by numerically solving the integration and differential equation shown in Equations (26) and (28), respectively, subject to the boundary condition shown in Equation (29). Since now $z(\sigma)$ is a function of σ, we use an integrated (α_{int}) value of α given by

$$\alpha_{\text{int}} = \int_0^x d\sigma\, \alpha(\lambda, z_0, z(\sigma)). \tag{32}$$

Table 5: Parameter values used for plots in Section 4.

	λ	z_0	z_*	σ_0	$\sigma_{\max}$	$x_{\max}$
	0.10	4.0	5	1.6	10	1.70
Figure 8	0.10	4.2	5	1.6	10	1.70
	0.10	4.4	5	1.6	10	1.70
	0.10	4.7	5	0.6	10	1.00
Figure 9	0.20	4.7	5	0.6	10	0.81
	0.30	4.7	5	0.6	10	0.68

Table 6: Parameter values used for plots in Section 5.

	λ	z_0	z_*	z_h	b	σ_0	$\sigma_{\max}$	$x_{\max}$
	0.10	4.0	5	10	0.40	1.7	10	1.7
Figure 10	0.10	4.0	5	8	0.50	1.7	10	1.7
	0.10	4.0	5	6	0.67	1.7	10	1.7
	0.10	4.7	5	10	0.94	0.7	10	1.00
Figure 11	0.20	4.7	5	10	0.94	0.7	10	0.91
	0.30	4.7	5	10	0.94	0.7	10	0.77

The differential equation in Equation (28) is numerically solved over the range of the variable σ from 0 to $\sigma_{\max}$. The parameters z_0, σ_0, and $z*$ satisfy the boundary condition defined in Equation (29). The data points are generated by varying the upper limit of the integration in Equations (26) and Equation (32) over the range 0 to $x_{\max}$. The values of all the parameter used in Figures 8 and 9 are shown in Table 5. Again we apply the same strategy for the finite temperature case to numerically solve Equations (30) and (31). The parameter values used in Figures 10 and 11 are summarized in Table 6.

7. Conclusion

In this paper, we studied the condition required for vacuum instability in a holographic theory with dilaton field for both zero and finite temperature cases. We started by considering a LFH metric background containing dilaton field. We followed the approach of Reference [2] while the significant difference between this work and other studies on Schwinger-like effect is that there is no explicit external field responsible for vacuum decay rather the field is within the metric that causes the vacuum decay.

Potential analysis has been considered at both zero temperature and finite temperature. In the zero temperature case, we have considered that in the near-boundary region, a larger value of the critical field should be obtained for pair production; in addition, the effect of scale parameter is to decrease the value of the critical field. Interestingly, far from the boundary region, this scale parameter has no effect. The critical field has the maximum value near the boundary region, and this maximum value decreases with increasing value of the scale parameter. Interestingly, far from the boundary region, the critical field becomes almost independent of the scale parameter. α is the ratio of dilaton field to its critical value, and we have found that there is a preferable region where the condition $\alpha \geq 1$ is obtainable almost irrespective of λ value. Also, α depends on probe brane position significantly.

During tunneling process at zero temperature, increasing scale parameter leads to diminishing the potential barrier, so although the pair production via Schwinger effect has not been started yet, pair creation according to tunneling process increases. In the current study, for pair creation via Schwinger effect, condition $\alpha \geq 1$ is not enough because we need λ to be large. Similar to the zero temperature case, at finite temperature also, α has its maximum value in the near-boundary region. In the region far from the boundary, α becomes independent of the temperature. The effect of scale parameter on α depends on the region completely, as the effect of scale parameter near the boundary is completely different with the near-horizon region. We found that the low-temperature region does not have a significant effect on the critical field, but at high temperature, the critical field falls down rapidly and with further increases in temperature, it becomes independent of the scale parameter. The results for the potential analysis at finite temperature is similar with the zero temperature case.

Pair production rate has been considered the exponential function of the action. We observe that in both zero temperature and finite temperature cases, the pair production rate decreases with increasing values of scale parameter and probe brane position. Also, the rate of decrease is rapid beyond the region $\alpha \geq 1$. So, in this work, although we observe vacuum instability under very restricted condition, there is no catastrophic pair production.

Data Availability

The data used to support the findings of this study are available from the corresponding author upon request.

Conflicts of Interest

The authors declare that they have no conflicts of interest.

Acknowledgments

This work was supported by the National Natural Science Foundation of China (Grant No. 11575254) and the National Key Research and Development Program of China (No. 2016YFE0130800). SN is supported by the China Postdoctoral Council under the International Postdoctoral Exchange Fellowship Program.

References

[1] J. Schwinger, "On gauge invariance and vacuum polarization," *Physical Review*, vol. 82, no. 5, pp. 664–679, 1951.

[2] Y. Sato and K. Yoshida, "Universal aspects of holographic Schwinger effect in general backgrounds," *Journal of High Energy Physics*, vol. 2013, no. 12, 2013.

[3] P. Jones, P. McDougall, and D. Singleton, "Particle production in a gravitational wave background," *Physical Review D*, vol. 95, no. 6, article 065010, 2017.

[4] Y. Sato and K. Yoshida, "Holographic description of the Schwinger effect in electric and magnetic field," *Journal of High Energy Physics*, vol. 2013, no. 4, p. 111, 2013.

[5] E. S. Fradkin and A. A. Tseytlin, "*Quantum string theory effective action*," *Nuclear Physics B*, vol. 261, pp. 1–27, 1985.

[6] C. Bachas and M. Porrati, "Pair creation of open strings in an electric field," *Physics Letters B*, vol. 296, no. 1-2, pp. 77–84, 1992.

[7] J. Maldacena, "The large N limit of superconformal field theories and supergravity," *International Journal of Theoretical Physics*, vol. 38, no. 4, pp. 1113–1133, 1999.

[8] E. Witten, "Anti de Sitter space and holography," *Advances in Theoretical and Mathematical Physics*, vol. 2, no. 2, pp. 253–291, 1998.

[9] S. S. Gubser, I. R. Klebanov, and A. M. Polyakov, "Gauge theory correlators from non-critical string theory," *Physics Letters B*, vol. 428, no. 1-2, pp. 105–114, 1998.

[10] O. Aharony, S. S. Gubser, J. Maldacena, H. Ooguri, and Y. Oz, "Large N field theories, string theory and gravity," *Physics Reports*, vol. 323, no. 3-4, pp. 183–386, 2000.

[11] A. Karch, E. Katz, D. T. Son, and M. A. Stephanov, "Linear confinement and AdS/QCD," *Physical Review D*, vol. 74, no. 1, article 015005, 2006.

[12] S. J. Brodsky and G. F. de Teramond, "AdS/CFT and QCD, slac-pub-12361," https://arxiv.org/abs/070220 [hepth].

[13] C. Csaki, M. Reece, and J. Terning, "The AdS/QCD correspondence: still undelivered," *Journal of High Energy Physics*, vol. 2009, no. 5, 2009.

[14] A. S. Gorsky, K. A. Saraikin, and K. G. Selivanov, "Schwinger type processes via branes and their gravity duals," *Nuclear Physics B*, vol. 628, no. 1-2, pp. 270–294, 2002.

[15] S. P. Kim, "Schwinger effect, Hawking radiation and gauge-gravity relation," *International Journal of Modern Physics A*, vol. 30, article 1545017, 2015.

[16] J. Ambjorn and Y. Makeenko, "Remarks on holographic Wilson loops and the Schwinger effect," *Physical Review D*, vol. 85, no. 6, article 061901, 2012.

[17] S. Bolognesi, F. Kiefer, and E. Rabinovici, "Comments on critical electric and magnetic fields from holography," *Journal of High Energy Physics*, vol. 2013, no. 1, p. 174, 2013.

[18] Y. Sato and K. Yoshida, "Holographic Schwinger effect in confining phase," *Journal of High Energy Physics*, vol. 2013, no. 9, p. 134, 2013.

[19] D. Kawai, Y. Sato, and K. Yoshida, "Schwinger pair production rate in confining theories via holography," *Physical Review D*, vol. 89, no. 10, article 101901, 2014.

[20] D. Kawai, Y. Sato, and K. Yoshida, "A holographic description of the Schwinger effect in a confining gauge theory," *International Journal of Modern Physics A*, vol. 30, no. 11, article 1530026, 2015.

[21] M. Sakaguchi, H. Shin, and K. Yoshida, "No pair production of open strings in a plane-wave background," *Physical Review D*, vol. 90, no. 6, article 066009, 2014.

[22] W. Fischler, P. H. Nguyen, J. F. Pedraza, and W. Tangarife, "Holographic Schwinger effect in de Sitter space," *Physical Review D*, vol. 91, no. 8, article 086015, 2015.

[23] K. Bitaghsir Fadafan and F. Saiedi, "On holographic non-relativistic Schwinger effect," *The European Physical Journal C*, vol. 75, p. 612, 2015.

[24] M. Ghodrati, "Schwinger effect and entanglement entropy in confining geometries," *Physical Review D*, vol. 92, no. 6, article 065015, 2015.

[25] U. N. Chowdhury, "Holographic description of noncommutative Schwinger effect," https://arxiv.org/abs/1904.09292.

[26] K. Hashimoto and T. Oka, "Vacuum instability in electric fields via AdS/CFT: Euler-Heisenberg Lagrangian and Planckian thermalization," *Journal of High Energy Physics*, vol. 2013, no. 10, p. 116, 2013.

[27] Y. Sato and K. Yoshida, "Potential analysis in holographic Schwinger effect," *Journal of High Energy Physics*, vol. 2013, no. 8, p. 2, 2013.

[28] G. W. Semenoff and K. Zarembo, "Holographic Schwinger effect," *Physical Review Letters*, vol. 107, no. 17, article 171601, 2011.

[29] S. J. Brodsky and G. F. de Teramond, "Light-front hadron dynamics and AdS/CFT correspondence," *Physics Letters B*, vol. 582, no. 3-4, pp. 211–221, 2004.

[30] S. J. Brodsky, G. F. de Téramond, H. G. Dosch, and J. Erlich, "Light-front holographic QCD and emerging confinement," *Physics Reports*, vol. 584, pp. 1–105, 2015.

[31] L. Zou and H. G. Dosch, "A very practical guide to light front holographic QCD," https://arxiv.org/abs/1801.00607.

[32] J. Sadeghi, B. Pourhassan, S. Tahery, and F. Razavi, "Holographic Schwinger effect with a deformed AdS background," *International Journal of Modern Physics A*, vol. 32, no. 10, article 1750045, 2017.

[33] O. Andreev, "$1/q^2$ corrections and gauge/string duality," *Physical Review D*, vol. 73, no. 10, article 107901, 2006.

[34] O. Andreev and V. I. Zakharov, "Heavy-quark potentials and AdS/QCD," *Physical Review D*, vol. 74, no. 2, article 025023, 2006.

[35] S. J. Rey and J. T. Yee, "Macroscopic strings as heavy quarks: large-N gauge theory and anti-de Sitter supergravity," *The European Physical Journal C*, vol. 22, no. 2, pp. 379–394, 2001.

[36] J. Maldacena, "Wilson loops in large N field theories," *Physical Review Letters*, vol. 80, no. 22, pp. 4859–4862, 1998.

[37] K. Hashimoto, T. Oka, and A. Sonoda, "Electromagnetic instability in holographic QCD," *Journal of High Energy Physics*, vol. 2015, no. 6, p. 1, 2015.